Journal of Power Sources 256 (2014) 220–225

Contents lists available at ScienceDirect

Journal of Power Sources

journal homepage: www.elsevier.com/locate/jpowsour

Raman diagnostics of $LiCoO_2$ electrodes for lithium-ion batteries

Toni Gross, Christian Hess*

Eduard-Zintl-Institut für Anorganische und Physikalische Chemie, Technische Universität Darmstadt, Alarich-Weiss-Str. 8, 64287 Darmstadt, Germany

HIGHLIGHTS

- Spatially-resolved analysis of $LiCoO_2$ electrodes shows chemical heterogeneity.
- *In situ* analysis of lithium de-intercalation of powder $LiCoO_2$ composite electrodes.
- Presence of resonance Raman effect for $LiCoO_2$ materials.
- *In situ* experiments demonstrate complementarity of XRD and Raman analysis.

GRAPHICAL ABSTRACT

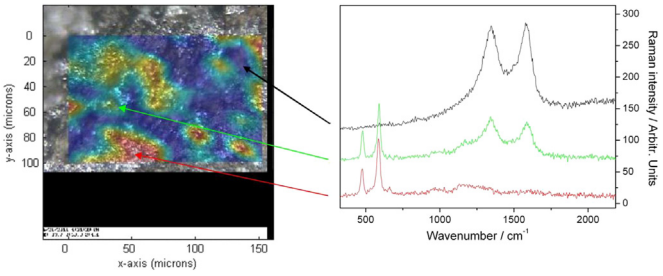

ARTICLE INFO

Article history:
Received 20 November 2013
Received in revised form
20 December 2013
Accepted 17 January 2014
Available online 24 January 2014

Keywords:
Lithium-ion batteries
$LiCoO_2$
In situ Raman spectroscopy
Spatially-resolved analysis
Resonance Raman

ABSTRACT

$LiCoO_2$ based electrode materials were characterized in detail using visible Raman spectroscopy. The studied materials comprise the active $LiCoO_2$ material itself as well as electrochemically relevant composites of $LiCoO_2$ with binder and conductive additives. Spatially resolved analysis, i.e. mapping of $LiCoO_2$ composite electrodes reveals a significant variation of chemical composition across the electrode surface. Based on wavelength-dependent studies we demonstrate the presence of a resonance enhancement for $LiCoO_2$ materials for green laser excitation allowing for *in situ* studies on the $LiCoO_2$-based electrodes during lithium de-intercalation. During *in situ* experiments no significant structural changes occur consistent with the fact that visible Raman spectroscopy probes mainly the surface region of the $LiCoO_2$ composite electrode. Our results demonstrate the potential of Raman spectroscopy for spatially resolved and *in situ* analysis of lithium-ion batteries.

1. Introduction

Secondary lithium-ion batteries are used for electrical energy storage in a variety of portable devices such as mobile phones and notebook computers or hybrid vehicles. Their application as power source in all-electric vehicles or grid energy storage is still hampered by the loss of electrochemical performance due to side reactions especially at the positive electrode [1]. A detailed understanding of the battery fatigue and rational design of improved lithium-ion batteries requires advances in electrode characterization and, in particular, the development of techniques suitable for monitoring the electrodes during battery operation. Raman spectroscopy is a non-destructive optical method, which allows probing the local structure of solid materials under various reaction environments. Previous studies have shown that Raman spectra can provide valuable information on secondary lithium-ion battery electrodes regarding e.g. phase identification, local order/disorder or spatially resolved composition (mapping) also under *in situ* and confocal conditions [2–14].

Very recent *in situ* X-ray absorption spectroscopy studies on the $LiCoO_2$ electrode/electrolyte interface have reported the irreversible reduction of Co^{3+} in the surface region (X-ray penetration depth ~3 nm) during the first charge/discharge process [15]. As a possible product of this process Co_3O_4 was postulated. Raman

* Corresponding author.
E-mail address: hess@pc.chemie.tu-darmstadt.de (C. Hess).

0378-7753/$ – see front matter © 2014 Elsevier B.V. All rights reserved.
http://dx.doi.org/10.1016/j.jpowsour.2014.01.084

spectroscopy has the potential to observe such species under *in situ* conditions. However, to increase the sensitivity of the method it would be highly desirable to explore the presence of resonance enhancements. Once established, best possible utilization of resonance effects for intensity increase will be accessible by using tunable laser excitation allowing to systematically probe the available parameter space of electronic excitations. So far only few studies have reported the presence of resonance Raman effects in Li ion battery cathode materials, i.e. $LiNi_xMn_{2-x}O_4$ [12], $LiNiCoO_x$ and $LiNiCoMnO_x$ [16]. $LiCoO_2$, which is among the most important active materials for cathodes, has been the subject of several Raman studies focusing mainly on phase identification via the A_{1g} and E_g phonon bands around 595 and 485 cm^{-1}, respectively [3–6,17,18]. However, neither a dependence on excitation wavelength nor the presence of resonance Raman effects have been reported.

In this contribution we describe a detailed Raman spectroscopic characterization of $LiCoO_2$ electrode materials. In the results and discussion section first the structure, then the resonance enhancement, and finally the spatially-resolved analysis and *in situ* analysis of powder $LiCoO_2$ electrode materials are described. The signal enhancement by resonance Raman scattering forms the basis for the spatially-resolved and *in situ* analysis described in the second half of the contribution.

2. Experimental

2.1. Synthesis

$LiCoO_2$ materials were prepared via a modified Pechini process. Cobalt nitrate (Merck, >99%) and lithium nitrate (Merck, >98%) were dissolved in water. Citric acid (Applichem, 98%) was added as complexation agent and the pH was adjusted to 5 by using 25% NH_3 solution. After addition of ethylene glycol the solution was heated to 180 °C for 6 h. The resulting black solid was ground, pre-calcined at 450 °C for 6 h, ground again and finally calcined at 800 °C for 20 h. Composite electrodes were prepared by thoroughly mixing the active material ($LiCoO_2$), carbon black (Timcal, Super P Li) and polyvinylidene difluoride (PVDF) (Solef, H 8048).

2.2. X-ray diffraction

X-ray powder diffraction (XRD) was performed on a Stadi-P diffractometer (STOE) in transmission geometry. The diffractometer is equipped with a molybdenum X-ray tube (Mo-$K_{\alpha 1}$ = 0.70926 Å), a curved Ge-(111)-monochromator and a linear position sensitive detector (PSD) with an aperture of 6°. Patterns were collected in an angular range of 7–50° (2θ) with a step width of 0.01° (2θ). Rietveld refinements for data analysis were done using the WINPLOTR software package [19].

2.3. Raman spectroscopy

Raman experiments were performed by using three visible excitation wavelengths, i.e. 514.5 nm from an argon ion laser (Melles Griot), 532 nm from a frequency-doubled Nd:YAG laser (Cobolt) and 632.8 nm from a He–Ne laser (Melles Griot). The scattered light was sent to a transmission spectrometer (Kaiser Optical, HL5R) equipped with an electrically cooled CCD detector with 256 × 1024 pixels. The elastically scattered light was blocked by SuperNotch Plus filters (Kaiser Optical). For calibration of the spectrometer emission lines of standard Ar and Ne lamps were used. The spectral resolution was 5 cm^{-1}; the wavelength stability was better than 0.5 cm^{-1}. The laser beam was focused onto the sample using a long-working 20 × objective. The laser power was set to 7 mW as measured with a power meter (Ophir) at the position of the sample. Mapping experiments were performed using a Microprobe (Kaiser Optical). The laser beam was focused onto the sample using a 100× objective. In these experiments the laser power was set to 1 mW at the sample.

In situ experiments were performed in 180° backscattering geometry using a home-built stainless steel cell with a sapphire optical window allowing for Raman experiments during electrochemical cycling (see Fig. 1). One half of the *in situ* cell was made of standard Swagelok parts. As Swagelok cells are commonly used as testing cells, the design of the cell was deduced from the standard cells, for better comparison with normal electrochemical data. The battery cell consists of two electrodes separated by several layers of glass fiber filter paper soaked with electrolyte to prevent a short circuit. Galvanostatic cycling was performed at a cycling rate of C/8 (corresponding to 64 mA g^{-1}) by using potential limits of E_{min} = 2.7 V and E_{max} = 4.2 V. As positive electrode a cathode mix (85% active material, 10% PVDF, 5% carbon black) with $LiCoO_2$ as active material was used; Li metal served as counter electrode. The electrolyte consisted of 1 M $LiClO_4$ dissolved in propylene carbonate.

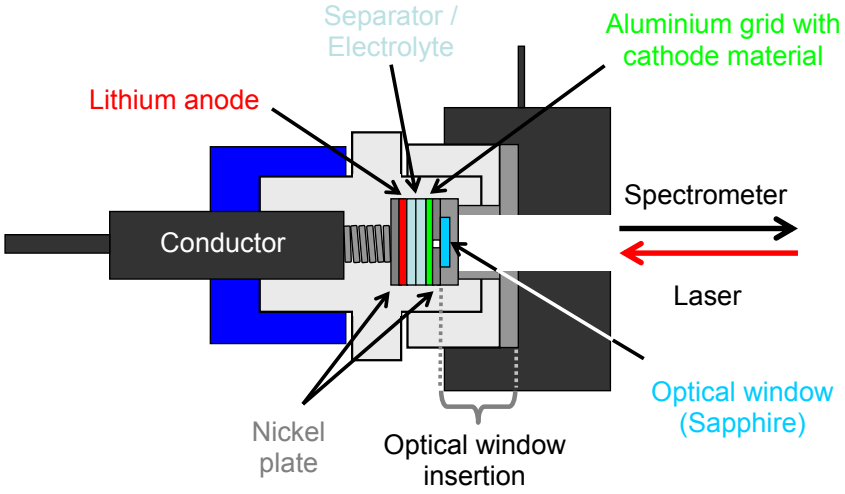

Fig. 1. Cross-sectional view of the *in situ* cell used for Raman diagnostics of $LiCoO_2$ electrodes.

3. Results and discussion

3.1. Structure

The structure of the $LiCoO_2$ samples was first investigated using X-ray diffraction (XRD). Fig. 2 shows the XRD patterns of as prepared $LiCoO_2$ (top panel) and composite $LiCoO_2$ (bottom panel) confirming the presence of a single phase of layered rock-salt $LiCoO_2$ (space group R-3m, number 166) with lattice parameters $a = 2.8152(4)$ Å and $c = 14.055(3)$ Å for as prepared $LiCoO_2$ and $a = 2.8163(2)$ Å and $c = 14.056(3)$ Å for composite $LiCoO_2$. The estimated standard deviations (in brackets) were calculated according to references [20,21]. Full pattern analysis of the obtained diffractograms shows no evidence of phase impurity. The structural model used gives the theoretical positions of reflections originating from the modeled phase (green markers). Only reflections from $LiCoO_2$ are observed. Likewise, the difference plots between calculated and measured data points (blue line) give no indication for impurity phase reflections.

Fig. 3 depicts the Raman spectra of as prepared $LiCoO_2$ (top panel) and composite $LiCoO_2$ (bottom panel) at 514 nm excitation. The Raman spectrum of hexagonal $LiCoO_2$ is characterized by two Raman bands at 595 and 485 cm^{-1}, respectively. Previously, these bands have been attributed to oxygen vibrations involving mainly Co–O stretching (A_{1g}) and O–Co–O bending (E_g) vibrations [4,17,22]. Besides, for the first time, a major feature is observed at around 1170 cm^{-1}, which is attributed to an overtone of the A_{1g} mode (see discussion below). In case of the composite $LiCoO_2$ additional broad Raman bands appear at around 1350 cm^{-1} and 1590 cm^{-1}. By comparison with the Raman spectrum of bare carbon black these features are readily attributed to carbon black; they are characteristic for the so-called defect band (D band) and C–C stretching mode (G band) of graphite, respectively [23,2]. The origin of the additional small feature at around 1000 cm^{-1} observed for as prepared $LiCoO_2$ is currently under study. However, the presence of spinel $LiCoO_2$ (LT-$LiCoO_2$) or Co_3O_4 can be ruled out [18,24].

3.2. Resonance enhancement

To gain insight into the sensitivity of Raman spectroscopy for $LiCoO_2$-based materials the laser excitation wavelength was varied. The left panel of Fig. 4 depicts 514.5 nm, 532 nm and 632.8 nm Raman spectra of as prepared $LiCoO_2$. Decreasing the excitation wavelength from 632.8 to 514.5 nm leads to a reversal of the 485

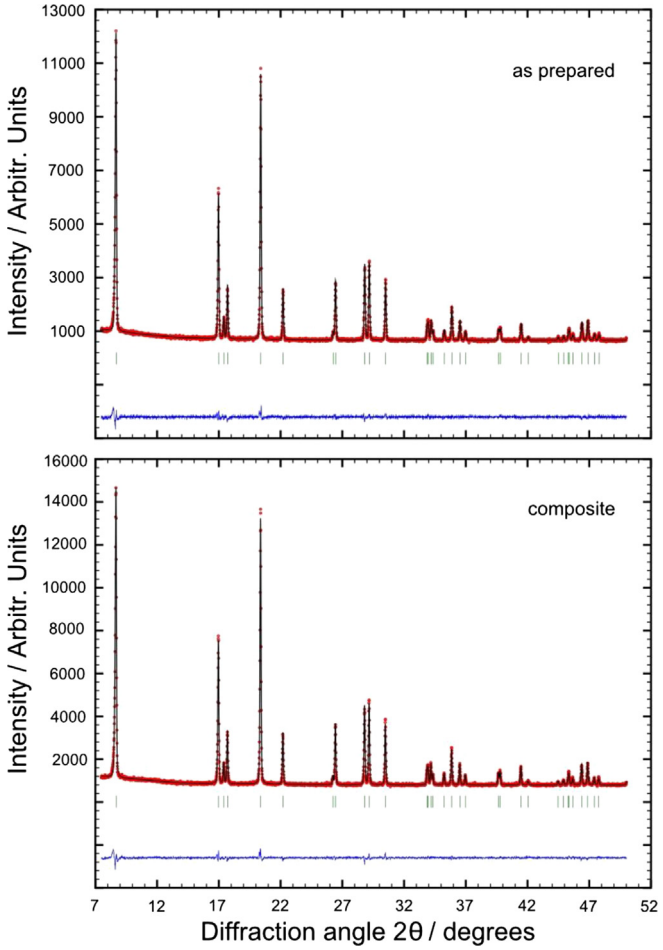

Fig. 2. XRD patterns of (top) as prepared $LiCoO_2$ and (bottom) composite $LiCoO_2$ (84% $LiCoO_2$, 8% carbon black, 8% PVDF). The lattice constants are $a = 2.8152(4)$ Å and $c = 14.055(3)$ Å for as prepared $LiCoO_2$ and $a = 2.8163(2)$ Å and $c = 14.056(3)$ Å for composite $LiCoO_2$. Green lines mark the positions of the reflections for the respective phase. Blue lines symbolize the difference plots between acquired and fitted data. (For interpretation of the references to color in this figure legend, the reader is referred to the web version of this article.)

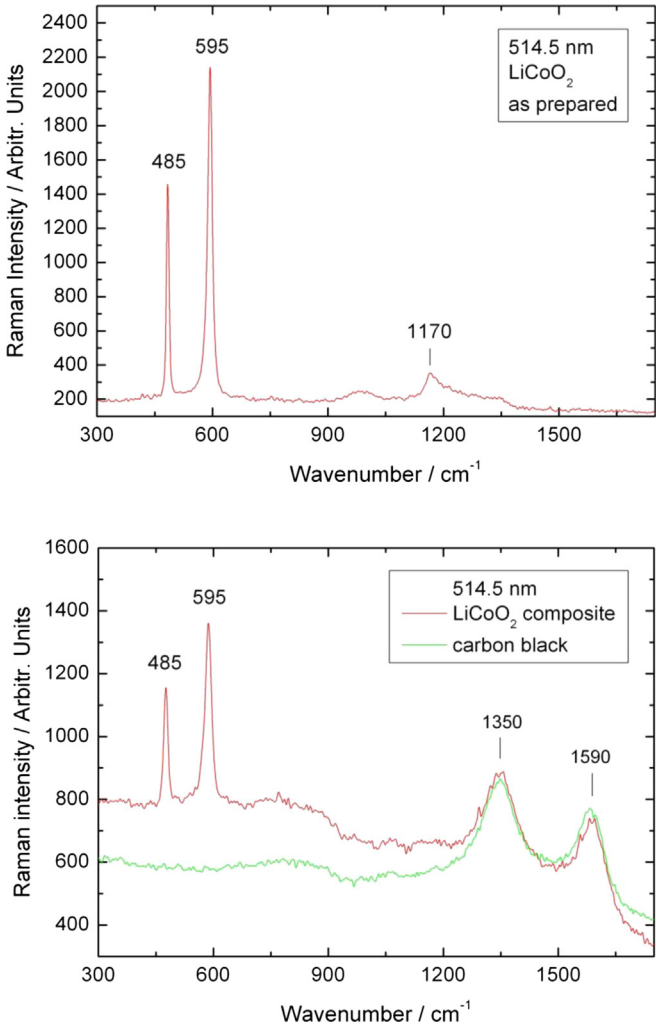

Fig. 3. Top panel: Raman spectrum of as prepared $LiCoO_2$ at 514 nm excitation. Bottom panel: 514 nm Raman spectrum of composite $LiCoO_2$ (84% $LiCoO_2$, 8% carbon black, 8% PVDF). For comparison a 514 nm Raman spectrum of bare carbon black is shown.

and 595 cm^{-1} band intensities and the appearance of a band at around 1170 cm^{-1} besides an improved signal-to-noise ratio. The latter as well as the overtone intensity show a slight increase upon switching from 514.5 nm to 532 nm excitation. The integrated intensities of the 485 cm^{-1} and the 595 cm^{-1} band after background subtraction for a series of experiments are shown in the right panel of Fig. 4. The A_{1g}/E_g intensity ratio increases from 0.9 to 2.3 when the excitation wavelength is changed from 632.8 nm to 532 nm and from 0.9 to 2.8 for a wavelength change from 632.8 nm to 514.5 nm. Is it known from the literature that $LiCoO_2$ possesses a prominent optical absorption at around 2.1 eV (591 nm) attributed to the d–d transition from Co-t2g to Co-eg bands [25]. Thus the observed behavior can be explained by the involvement of this electronic transition in a resonance enhancement process. The presence of resonance Raman scattering is corroborated by the selective enhancement of the A_{1g} mode as well as the occurrence of the overtone of the A_{1g} mode at around 1170 cm^{-1}. With respect to the overall wavelength dependence observed the following qualitative picture can be drawn: in case of 632.8 nm excitation the frequency is too small to cause resonance. In contrast, for 514.5 nm and 532 nm excitation, the frequency is sufficiently close to that of the t2g-eg electronic transition for resonance Raman scattering to occur. A similar behavior has been observed by Bosworth et al. for transition metal complexes [26]. Please note that the above interpretation resolves the literature issue of different relative intensities of the E_g and A_{1g} bands obtained by 632.8 nm and 514.5 nm excitation [24,4].

Fig. 5 demonstrates the presence of the resonance Raman effect under electrochemical conditions. To this end the cathode composite (85% $LiCoO_2$, 10% PVDF, 5% carbon black) was studied in the presence of electrolyte consisting of 1 M $LiClO_4$ dissolved in propylene carbonate i.e. under *in situ* conditions. The spectra are characterized by the two Raman bands at 485 (486) and 595 (596) cm^{-1} as discussed above. Switching the laser excitation wavelength from 632.8 nm to 514.5 nm results in a reversal of the A_{1g}/E_g intensity ratio. The values for the A_{1g}/E_g intensity ratio change from 0.83 (632.8 nm) to 2.96 (514.5 nm) consistent with the values given in the right panel of Fig. 4. Thus we can conclude that the resonance Raman effect observed for the as prepared samples is preserved under electrochemical conditions.

Besides the phonon bands, the spectra exhibit broad carbon-related bands at around 1350 cm^{-1} (D band) and 1590 cm^{-1} (G band) originating from the carbon black additive (see discussion above). In case of 632.8 nm excitation the D band is largely covered by two strong features at 1369 and 1399 cm^{-1} due to the sapphire windows of the *in situ* cell. These luminescence features originate from transition metal impurities in α-Al_2O_3, which are excited at

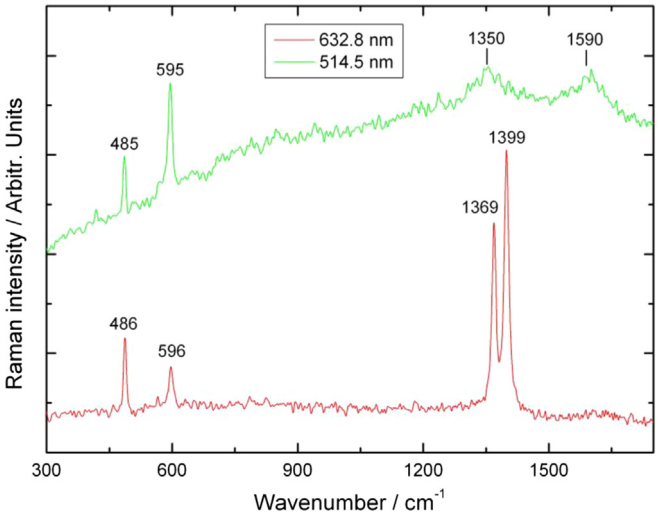

Fig. 5. *In situ* Raman spectra of the cathode composite (85% $LiCoO_2$, 10% PVDF, 5% carbon black) using 514.5 nm and 632.8 nm laser excitation. Spectra were offset for clarity. For details see text.

632.8 nm but not at 514.5 nm. At 514.5 nm excitation minor features at 715, 850 and 930 cm^{-1} are observed, which are associated with the electrolyte. Their detailed assignments will be discussed below (see. Figs. 7 and 8). In addition, at 514.5 nm laser excitation, the presence of propylene carbonate gives rise to two Raman features at 2940 and 2990 cm^{-1} attributed to CH_3 stretching modes (not shown).

Based on the signal enhancement by resonance Raman scattering spatially-resolved and *in situ* analysis during lithium de-intercalation has been performed as described in the following.

3.3. Spatially-resolved analysis

The left part of Fig. 6 shows a Raman mapping as a result of a spatially resolved Raman analysis of a $LiCoO_2$ cathode composite covering an area of 100 μm × 150 μm. To this end, the individual Raman spectra were analyzed regarding the intensities of the 595 cm^{-1} phonon band and the sum of the D and G carbon bands. In Fig. 6, the integrated intensities are overlayed onto the microscopy image of the area under study. The mapping data demonstrates the heterogeneity of the chemical composition along the $LiCoO_2$ composite. The distribution of $LiCoO_2$ (top left image) and carbon (bottom left image) is complementary; there is no

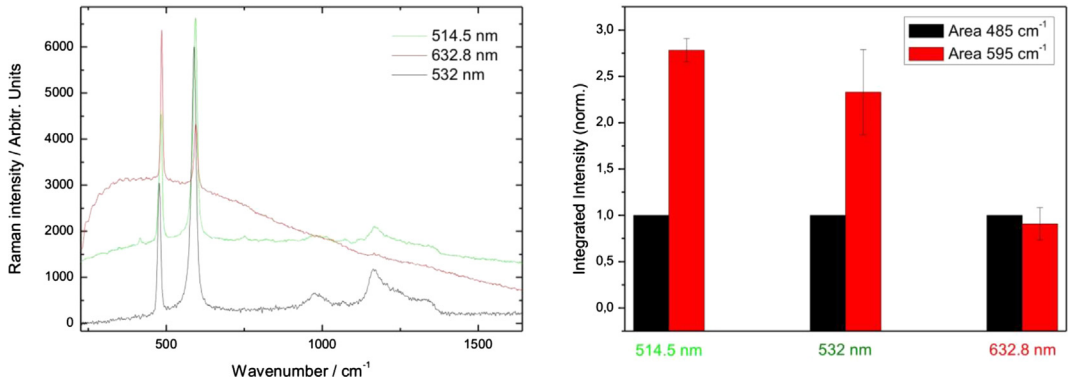

Fig. 4. Left panel: Raman spectra of as prepared $LiCoO_2$ using 514.5 nm, 532 nm and 632.8 nm laser excitation. Right panel: Integrated intensities of the 485 cm^{-1} and the 595 cm^{-1} band after background subtraction for a series of measurements.

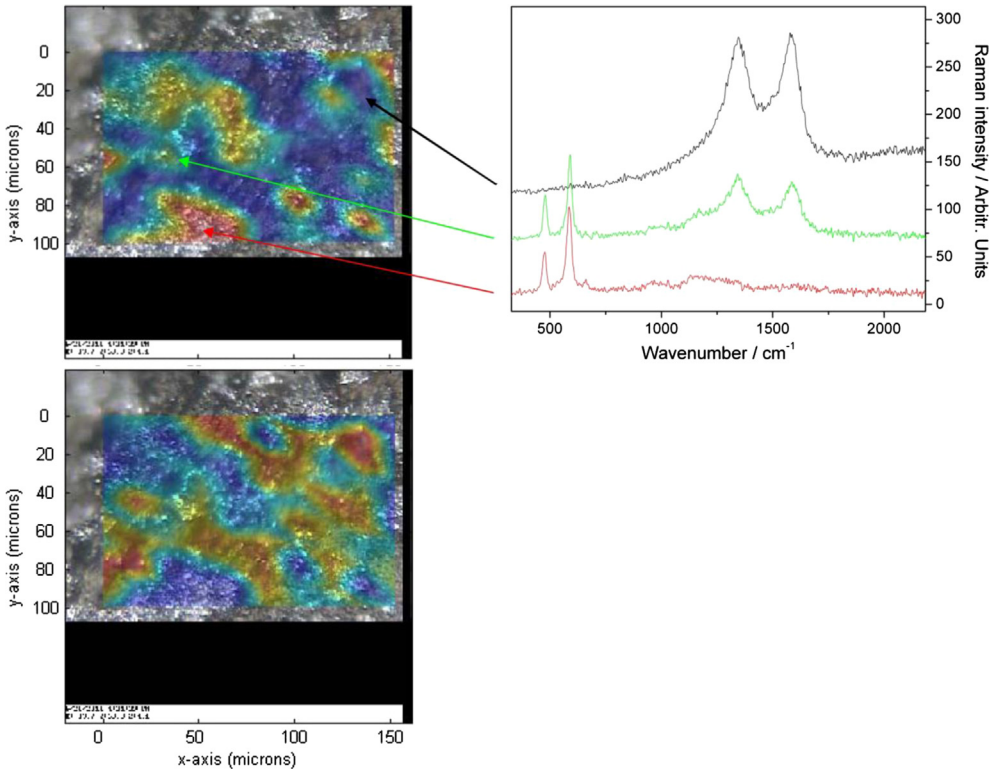

Fig. 6. Raman mapping of a cathode composite (85% $LiCoO_2$, 10% PVDF, 5% carbon black) overlayed onto the corresponding microscopy image showing the $LiCoO_2$ (top left image) and carbon (bottom left image) distribution. The Raman spectra on the right correspond to the indicated points of the Raman map. Laser excitation at 532 nm was used. Spectra were offset for clarity. For details see text.

indication for PVdF related Raman signals. The individual active mass particles vary in size but are typically in the range of ~10–20 μm. Besides, comparison of the mapping data with the microscopy image shows a correlation of the chemical distribution with the surface topology. Individual Raman spectra from different locations of the analyzed area are depicted in the right part of Fig. 6. The spectra were chosen to display the spectrum of chemical compositions present at the surface of the $LiCoO_2$ composite. $LiCoO_2$ and carbon band assignments have been discussed above. Summarizing, the results in Fig. 6 underline the potential of Raman spectroscopy for spatially resolved analysis of $LiCoO_2$ composite materials allowing for detection of single active mass particles.

3.4. *In situ* experiments during lithium de-intercalation

There are only few *in situ* Raman studies on $LiCoO_2$ materials during lithium de-intercalation. These comprise the work by Itoh et al. and Kuwata et al. on thin film electrodes prepared on gold and Pt/SiO2 substrates, respectively [5,27]. So far no *in situ* Raman studies during de-intercalation of powder $LiCoO_2$ composite electrodes have been reported despite their relevance. Exploiting the enhancement by resonance Raman scattering Fig. 7 shows *in situ* spectra during de-intercalation of $LiCoO_2$ composite electrode. The $Li_{1-x}CoO_2$ composite was de-intercalated in steps of $\Delta = 0.1$ (10%). The electrolyte consisted of 1 M $LiClO_4$ dissolved in propylene carbonate. The inset displays the corresponding electrochemical data. The spectra are characterized by the two Raman bands at 485 and 595 cm^{-1} discussed above. In addition, minor features at 715, 850 and 930 cm^{-1} are observed, which are assigned to skeletal bending, symmetric ring and O–(C=O)–O symmetric stretching vibrations of the propylene carbonate solvent, respectively [28,29]. This assignment is supported by the Raman spectrum of the electrolyte, i.e. 1 M $LiClO_4$ in propylene carbonate, which shows sharp characteristic bands at 712, 850, 933, 959 and 1089 cm^{-1} (see Fig. 8). While a detailed look at the spectrum of the $LiCoO_2$ composite electrode in Fig. 7 indicates the presence of small feature at around 960 cm^{-1}, the electrolyte band at 1089 cm^{-1} is covered by the increasing background. The presence of propylene carbonate

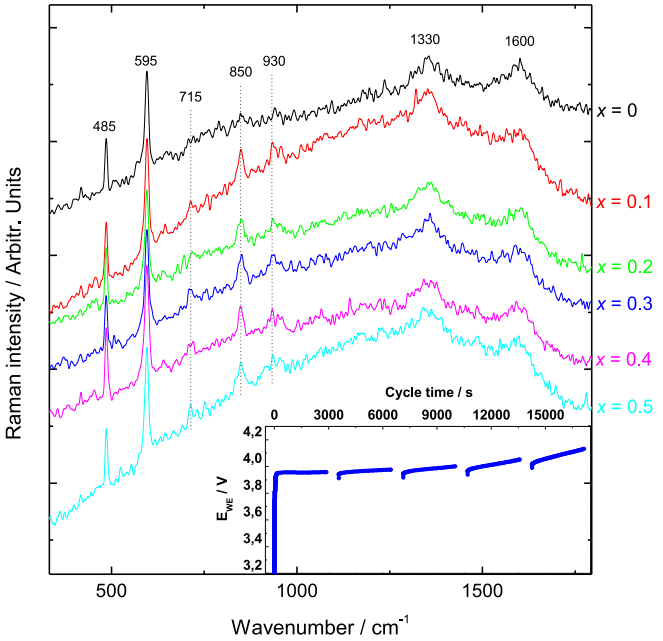

Fig. 7. *In situ* Raman spectra of a $Li_{1-x}CoO_2$ composite (85% $LiCoO_2$, 10% PVDF, 5% carbon black) during Li de-intercalation using 514 nm laser excitation. Spectra were offset for clarity. The inset displays the corresponding electrochemical data. Each step corresponds to the extraction of 10% of Li. The relaxation time between de-intercalation steps is 690 s.

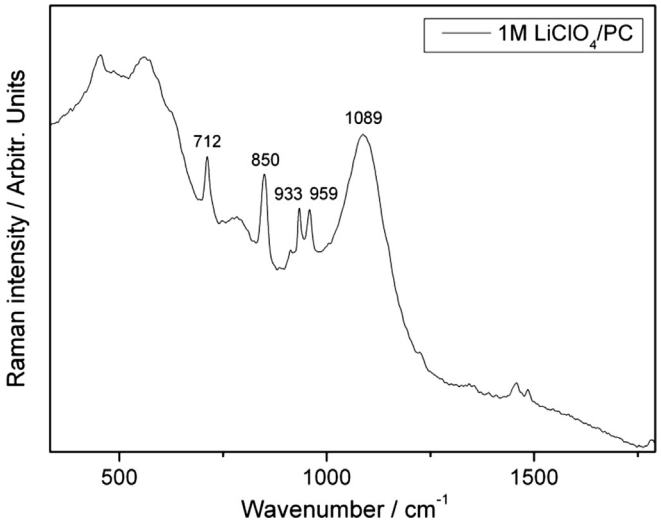

Fig. 8. Raman spectrum of 1 M $LiClO_4$ dissolved in propylene carbonate.

gives rise to two other Raman bands at 2940 and 2990 cm^{-1} attributed to CH_3 stretching modes (not shown). The occurrence of electrolyte signals strongly indicates that the electrode is fully immersed in the electrolyte during experiments. Besides, all spectra exhibit broad carbon-related bands at around 1330 cm^{-1} (D band) and 1600 cm^{-1} (G band) originating from the carbon black additive.

From the *in situ* data presented here there is no indication of significant structural changes during lithium de-intercalation. On the other hand, previous *in situ* XRD on $LiCoO_2$ electrodes have shown a change in the *c* parameter during de-/intercalation [30]. This suggests that, due to the limited penetration depth of visible radiation, visible Raman spectroscopy probes mainly the surface region of the $LiCoO_2$ composite electrodes, which in contrast to the bulk of the active mass particles does not undergo structural changes. In this respect *in situ* Raman spectroscopy gives complementary information to *in situ* XRD. The elucidation of the origin of degradation of $LiCoO_2$-based electrode materials is still under debate. To this end, Raman spectroscopy is expected to contribute to this discussion in the future due to its potential to deliver spatially resolved and *in situ* information.

4. Conclusions

The visible Raman spectra of $LiCoO_2$-based electrode materials were investigated in detail in their as prepared state, as composite with binder and conductive additives as well as under *in situ* conditions. Wavelength-dependent studies have revealed the presence of resonance Raman scattering for green laser excitation due to changes of the A_{1g} and E_g intensity ratio and the occurrence of an overtone of the A_{1g} band. Based on the signal enhancement spatially-resolved and *in situ* analysis has been performed. Raman mapping of $LiCoO_2$ composite materials reveals a significant variation of chemical composition and active mass particles of ~10–20 μm in size. *In situ* experiments show that visible Raman spectroscopy probes mainly the surface region of the $LiCoO_2$ composite electrode, which is not subject to significant structural changes during lithium de-intercalation.

Acknowledgments

This work was supported by SFB595 of the Deutsche Forschungsgemeinschaft (DFG). The authors thank Lars Giebeler and Julia Eigenseer for help with some of the Raman experiments and Karl Kopp for technical support. We like to thank Wolfgang Donner for the opportunity to carry out XRD measurements on the Stadi-P diffractometer.

References

[1] J.B. Goodenough, Acc. Chem. Res. (2012), http://dx.doi.org/10.1021/ar2002705.
[2] R. Baddour-Hadjean, J.-P. Pereira-Ramos, Chem. Rev. 110 (2010) 1278.
[3] P. Novak, J.C. Panitz, F. Joho, M. Lanz, R. Imhof, M. Coluccia, J. Power Sources 90 (2000) 52.
[4] M. Inaba, Y. Iriyama, Z. Ogumi, Y. Todzuka, A. Tasaka, J. Raman Spectrosc. 28 (1997) 613.
[5] T. Itoh, H. Sato, T. Nishina, T. Matue, I. Uchida, J. Power Sources 68 (1997) 333.
[6] T. Itoh, N. Anzue, M. Mohamedi, Y. Hisamitsu, M. Umeda, I. Uchida, Electrochem. Commun. 2 (2000) 743.
[7] Y. Luo, W.-B. Cai, X.-K. Xing, D.A. Scherson, Electrochem. Solid-State Lett. 7 (2004) E1.
[8] J. Lei, F. McLarnon, R. Kostecki, J. Phys. Chem. B 109 (2005) 952.
[9] W. Huang, R. Frech, J. Power Sources 81–82 (1999) 616.
[10] K. Dokko, Q. Shi, I.C. Stefan, D.A. Scherson, J. Phys. Chem. B 107 (2003) 12549.
[11] Q. Shi, Y. Takahashi, J. Akimoto, I.C. Stefan, D.A. Scherson, Electrochem. Solid-State Lett. 8 (2005) A521.
[12] K. Dokko, M. Mohamedi, N. Anzue, T. Itoh, I. Uchida, J. Mater. Chem. 12 (2002) 3688.
[13] K. Dokko, N. Anzue, M. Mohamedi, T. Itoh, I. Uchida, Electrochem. Commun. 6 (2004) 384.
[14] P. Novak, D. Goers, L. Hardwick, M. Holzapfel, W. Scheifele, J. Ufheil, A. Würsig, J. Power Sources 146 (2005) 15.
[15] D. Takamatsu, Y. Koyama, Y. Orikasa, S. Mori, T. Nakatsutsumi, T. Hirano, H. Tanida, H. Arai, Y. Uchimoto, Z. Ogumi, Angew. Chem. 124 (2012) 11765.
[16] M. Kerlau, M. Marcinek, V. Srinivasan, R. Kostecki, Electrochim. Acta 52 (2007) 5422.
[17] C. Julien, Solid State Ionics 136–137 (2000) 887.
[18] L. Mendoza, R. Baddour-Hadjean, M. Cassir, J.P. Pereira-Ramos, Appl. Surf. Sci. 225 (2004) 356.
[19] T. Roisnel, J. Rodriguez-Carvajal, Mater. Sci. Forum 378–381 (2001) 118.
[20] J.F. Berar, P. Lelann, J. Appl. Crystallogr. 24 (1991) 1.
[21] J.F. Berar, Acc. in Pow. Diff. II, NIST Spec. Publ. 846, 1992, p. 63.
[22] M. Inaba, Y. Todzuka, H. Yoshida, Y. Grincourt, A. Tasaka, Y. Tomida, Z. Ogumi, Chem. Lett. 24 (1995) 889.
[23] F. Tuinstra, J. Chem. Phys. 53 (1970) 1126.
[24] E. Markevich, G. Salitra, D. Aurbach, Electrochem. Commun. 7 (2005) 1298.
[25] K. Kushida, K. Kuriyama, Solid State Commun. 118 (2001) 615.
[26] Y. Bosworth, R.J.H. Clark, J. Chem. Soc. Dalton Trans. (1974) 1749. In this paper the enhancement in Raman signal based on an excitation wavelength located within the tail of an electronic band is referred to as a pre-resonance effect.
[27] N. Kuwata, K. Ise, Y. Matsuda, J. Kawamura, T. Tsurui, O. Kamishima, Proceedings of the 13th Asian Conference on Solid State Ionics, Ionics for Sustainable World, World Scientific (2012) 138.
[28] G. Janz, J. Ambrose, J. Coutts, J. Downey Jr., Spectrochim. Acta Part A 35 (1979) 175.
[29] D. Battisti, G.A. Nazri, B. Klassen, R. Aroca, J. Phys. Chem. 97 (1993) 5826.
[30] S. Laubach, S. Laubach, P.C. Schmidt, D. Ensling, S. Schmid, W. Jaegermann, A. Thißen, K. Nikolowski, H. Ehrenberg, Ehrenberg, Phys. Chem. Chem. Phys. 11 (2009) 3278.